JOURNAL OF MATERIALS SCIENCE 41 (2006) 163–175

A Monte Carlo simulation on domain pattern and ferroelectric behaviors of relaxor ferroelectrics

J.-M. LIU*
Laboratory of Solid State Microstructures, Nanjing University, Nanjing 210093, China
E-mail: liujm@nju.edu.cn

S. T. LAU, H. L. W. CHAN, C. L. CHOY
Department of Applied Physics, The Hong Kong Polytechnic University, Hung Hom, Kowloon, Hong Kong, China

The domain configuration and ferroelectric property of mode relaxor ferroelectrics (RFEs) are investigated by performing a two-dimensional Monte Carlo simulation based on the Ginzburg-Landau theory on ferroelectric phase transitions and the defect model as an approach to the electric dipole configuration in relaxor ferroelectrics. The evolution of domain pattern and domain wall configuration with lattice defect concentration and temperature is simulated, predicting a typical two-phase coexisted microstructure consisting of ferroelectric regions embedded in the matrix of a paraelectric phase. The diffusive ferroelectric transitions in terms of the spontaneous polarization hysteresis and dielectric susceptibility as a function of temperature and defect concentration are successfully revealed by the simulation, demonstrating the applicability of the defect model and the simulation algorithm. A qualitative consistency between the simulated results and the properties of proton-irradiated ferroelectric copolymer is presented.

1. Introduction

The role of defects in ferroelectrics (FEs) has been one of the fundamental issues in physics of ferroelectrics. While most studies related to defects in ferroelectrics deal with domain boundary, twin structure, anti-phase boundary and dislocations etc, a comprehensive knowledge of these defects and their impact on the materials property would be important for materials processing and property optimization [1, 2]. Here, we focus on a special type of crystal defects which are believed to be responsible for the relaxor-like behaviors in some doped ferroelectrics [3–12]. These defects can be either impurity atoms distributed randomly in the lattice or off-center dopant ions which generate the so-called internal random fields or random bonds, or even a frustration of long-range ordering state due to some reasons [9]. Although it remains challenging to identify directly the core configuration and physical behaviors of these defects, extensive studies on relaxor ferroelectrics (RFEs) have provided a sound basis for establishing the essential roles of these defects [7–16]. Therefore, it becomes natural to correlate the existence of lattice defects with the abnormal ferroelectric and dielectric behaviors in RFEs.

It is well known that RFEs exhibit some features not often observed in normal FEs, such as diffusive phase transitions, strong frequency dependence of dielectric susceptibility which corresponds to a broad spectrum of electric-dipole relaxation times, narrow and frequency-dependent hyeteresis in the paraelectric state and weak FE-hysteresis below the FE transition point (Curie point) T_c, in addition to the high dielectric constant and excellent electromechanical performance [3, 4]. It is now believed that these abnormal behaviors are related to the coexistence of two phases in the nano-scale, i.e. well aligned dipolar micro-regions embedded in a matrix of paraelectric (PE) phase upon a decrease of temperature T towards T_c [14–16]. Such a picture of two-phase coexistence was employed in several models to explain the abnormal property of RFEs. The well-documented models include the compositional

*Author to whom all correspondence should be addressed.
0022-2461
DOI: 10.1007/s10853-005-6016-3

inhomogeneity scheme [17], the superparaelectric model [3], and the dipole-glass model [15], which describe the dipole-configuration of RFEs in a framework of standard dipole interactions coupled with an internal random field.

The role of defects mentioned above is considered in the compositional inhomogeneity model in which the type of defects can be impurity atom or dopant ion [12]. For the former, the impurity atoms in the lattice are viewed as disordered (random) static defects coupled locally with the transformational mode which is responsible for a stable dipole. Therefore, the defects may change the magnitude of local dipoles from site to site, by suppressing the dipole moment. For the latter, a model was proposed by Vugmeister *et al*. [9], where a highly polarizable PE host lattice with a displacive dielectric response to electric field E is considered. If this lattice is doped by off-center dopants, a local dipole will appear and the local dopant may occupy one of the crystallographically equivalent off-center sites around the unit cell center, and the resultant dipole moment may align along one of the equivalent vectors. Here it should be pointed out that the off-center displacement would lead to either a suppression or an enhancement of local dipole moment. Thus a consideration of two types of defects in lattice may be necessary: those defects that would suppress local dipoles magnitude (type-I) and those that may suppress or enhance local dipoles in a random manner (type-II). While there is not much direct evidence on the defects associated with the random-field scheme, some interesting experiments on ferroelectric copolymers had been performed recently, where the material was irradiated by ions such that the system was converted from a normal FE phase into two coexisting phases: a normal FE and a RFE phase [18–20]. The irradiated regions may lose their ferroelectricity and can be viewed as containing induced defects.

Recently, a thermodynamic description of the FE lattice with impurity-induced defects was developed by Su *et al*. [12] and Semenovskaya *et al*. [21], who included the effect of local dipole fluctuations induced by impurity ions in the Landau energy. Furthermore, the two-phase coexisted pattern may also depend on mechanisms other than defects, such as the long-range dipole-dipole interaction, gradient energy due to alignment misorientation and long-range elastic interaction [21]. It is necessary to consider these mechanisms in the theoretical approach.

In this paper, we summarize our recent Monte Carlo (MC) simulation on the lattice configuration of electric dipoles and the dielectric property in a FE lattice with local lattice defects [22–24]. The defects coupled into the lattice are identified as two types as mentioned above: one type is those intended to suppress the local dipoles (type-I) and the other supposed to suppress or enhance the dipoles in a random manner (type-II). The effect of both types of defects on the domain configurations and dielectric (ferroelectric) behaviors of RFEs will be simulated. We shall then compare our simulations on the effect of type-I defects with the experimental data on proton-irradiated poly (vinylidene fluoride-trifluoroethylene) 70/30 mol% copolymer (P(VDF-TrFE)) [25]. The reason is clear, since the proton-irradiation results in suppression of electric dipole.

The remaining part of this paper is organized as follows. In Section 2 the thermodynamic model on a defective ferroelectric lattice system with a cubic (square)-tetragonal (rectangle) ferroelectric transition upon temperature decreasing will be presented, followed by the MC-algorithm of simulation. The main results of the simulation and discussion on the significant effect of the two types of defects on the domain configuration and ferroelectric (dielectric) property of the lattice will be given in Section 3 to Section 5, followed by a short conclusion in Section 6.

2. Model and procedure of simulation

The MC simulation is performed on a two-dimensional (2D) $L\times L$ lattice with the periodic boundary conditions applied, where the PE phase takes the square configuration and FE phase the rectangular one. Basically, a three-dimensional lattice with a cubic-tetragonal transition should be employed for a reliable simulation, however, the computational capacity required for such a simulation is extremely big. Moreover, because we do not focus much on the critical phenomena associated with the ferroelectric phase transitions, the effect of finite lattice size may not be significant here to invalidate the main conclusion from the 2D simulation. We once employed a $16\times16\times16$ cubic lattice for a pre-simulation and did not find significant difference of the simulated results (e.g. dielectric susceptibility and ferroelectric property to be defined below) from those we obtained for a 2D lattice of $L\sim64$. In Fig. 1 we present the simulated dielectric susceptibility as a function of temperature T for a 3D lattice with $L = 16$, and two 2D lattices with $L = 64$ and 128, respectively. No significant difference between the several lattices is found in terms of the dielectric behavior. Therefore, all of our simulations reported below will be performed on a 2D lattice. Although the lattice for copolymer P(VDF-TrFE) cannot be viewed as a square in a strict sense, the thermodynamic approach may not be sensitive to the crystal symmetry and details of the lattice structure. Therefore, we ignore the crystallographic difference when we compare the simulated results with the experiments.

2.1. Ginzburg-Landau model of normal ferroelectric lattice

The model starts from the Ginzburg-Landau approach to normal ferroelectric lattice with a square-rectangle transition. For each lattice site, a dipole vector $\boldsymbol{P}$ is imposed with its moment and orientation defined by the energy

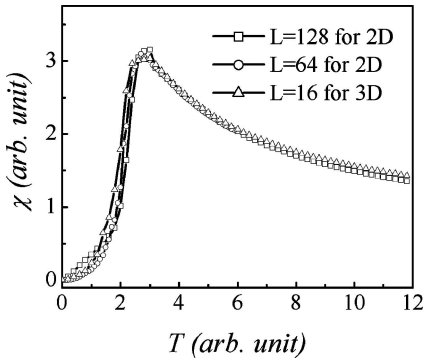

Figure 1 Simulated dielectric susceptibility as a function of temperature T for three lattices (3D lattice with $L = 16$, 2D lattices with $L = 64$ and 128, respectively). $Q = 4$. For details see text.

minimization. We define $\boldsymbol{P} = (P_x(\mathbf{r}), P_y(\mathbf{r}))$ where P_x and P_y are the two components along x-axis and y-axis, respectively. For the energy, we consider the contributions from the Landau double-well potential, the long-range dipole-dipole interaction and gradient energy associated with domain walls. For normal FE crystals the ferroelastic property can not be ignored [26]. However, this effect may not be important for a two-phase coexisted lattice like RFEs, because the actual dipole-ordered regions are nanometers in size and well-separated by the surrounding paraelectric phase whose elastic energy can be ignored.

The Landau double-well potential f_L can be written as [26]:

$$f_L(P_i) = A_1\left(P_x^2 + P_y^2\right) + A_{11}\left(P_x^4 + P_y^4\right) + A_{12}P_x^2P_y^2 + A_{111}\left(P_x^6 + P_y^6\right) \quad (1)$$

where subscript i refers to lattice site i, A_1, A_{11}, A_{12} and A_{111} are the energy coefficients, respectively. For normal FEs, $A_1 > 0$ favors a stable or meta-stable PE phase while a first-order ferroelectric transition will occur if $A_1 < 0$. In fact, one has $A_1 = 1/2\varepsilon_0\chi$ for the PE phase where ε_0 is the vacuum permitivity and χ the dielectric susceptibility of the local lattice. In the present model, the dipole vector is assumed to take one of Q orientations, where Q is treated as a variable. For a square-rectangle transition considered here, $Q = 4$ if one only looks at the Landau energy. However, other orientation states may be chosen too if other dipole interactions are considered. Each dipole is determined by the energy minimization. We shall simulate the effect of Q on the domain configuration, but in most cases we choose Q=4, i.e. four equivalent orientations: [1, 0], [−1, 0], [0, 1] and [0, −1] are allowed, where orientation [1, 0] refers to the horizontal-right x-axis, and [0, 1] refers to the vertical-up y-axis.

If there exists a spatial distribution of the dipoles (refer to either moment or orientation), an additional energy is generated, i.e. the so-called gradients of the polarization field induced by the fluctuation. For a 2D lattice, it can be written as [21, 26]:

$$f_G(P_{i,j}) = \frac{1}{2}G_{11}\left(P_{x,x}^2 + P_{y,y}^2\right) + G_{12}P_{x,x}P_{y,y} + \frac{1}{2}G_{44}(P_{x,y} + P_{y,x})^2 + \frac{1}{2}G'_{44}(P_{x,y} - P_{y,x})^2 \quad (2)$$

where $P_{i,j} = \partial P_i/\partial x_j$. Since parameters G_{11}, G_{12}, G_{44} and G'_{44} are all positive, in most cases this energy term is positive, which means that any dipole fluctuation either in moment or in orientation is not favored. The role of this gradient term is obviously opposite to that of the dipole-dipole interaction to be described below, i.e. ferroelectric ordering is preferred by this term. In addition, the dipole-dipole interaction is long-ranged and it should be considered for an inhomogeneous system. In the SI unit, the energy for site i can be written as [26]:

$$f_{\text{dip}}(P_i) = \frac{1}{8\pi\varepsilon_0\chi}\sum_{\langle j\rangle}\left[\frac{P(r_i)\cdot P(r_j)}{|r_i - r_j|^3} - \frac{3[P(r_i)\cdot(r_i - r_j)][P(r_j)\cdot(r_i - r_j)]}{|r_i - r_j|^5}\right] \quad (3)$$

where $\langle j\rangle$ represents a summation over all sites within a circle region centered at site i with radius R, parameters r_i, r_j, $P(r_i)$ and $P(r_j)$ here should be vectors, r_i and r_j are the coordinates of sites i and j, respectively. In a strict sense, R should be infinite but an effective cut-off at $R = 8$ is taken in our simulation (the as-induced error from this cut-off is less than 2% in terms of the relative accuracy). The total dipole-dipole interaction energy for the whole lattice can be written in the integration form:

$$F_{\text{dip}} = \int d^3r_i\, f_{\text{dip}}(P_i) = \frac{1}{8\pi\varepsilon_0\chi}\int\int^3 r_i d^3r_j\left[\frac{P(r_i)\cdot P(r_j)}{|r_i - r_j|^3} - \frac{3[P(r_i)\cdot(r_i - r_j)][P(r_j)\cdot(r_i - r_j)]}{|r_i - r_j|^5}\right] \quad (4)$$

It is clearly seen that a minimizing of F_{dip} favors the alignment of dipoles in the head-to-tail form. The energy for an anti-parallel dipole alignment between two neighboring rows is slightly lower than that for a parallel alignment between the two rows. A compatible competition between f_{dip} and f_G is responsible for dominance of either 90°-domain walls or 180°-walls. When f_{dip} is slightly larger than f_G, 180°-walls dominate. Finally, the

electrostatic energy induced by an external electric field is:

$$f_E(P_i) = -P_i \cdot E \tag{5}$$

where E is external electric field, and P_i and E are vectors. In our simulation, vector E takes the [1, 0] direction. The Hamiltonian for the system is:

$$H = \sum_{<i>} f_L + f_G + f_{\text{dip}} + f_E \tag{6}$$

where $<i>$ refers to the summation over the whole lattice.

2.2. Effect of defects

Introduction of randomly distributed defects imposes a spatial distribution for the coefficients A_1, A_{11}, A_{12} and A_{111} in the Landau energy Equation 1. Consequently, the other three terms become defect-dependent too. We also assume that only A_1 is affected by the defects and the other three coefficients remain unchanged [21]. That is:

$$\begin{aligned} A_1(r_i) &= A_{10} + b_m \cdot c \\ A_{10} &= \alpha(T - T_0), \quad \alpha > 0 \end{aligned} \tag{7}$$

where $\alpha > 0$ is a materials constant, T is the temperature, A_{10} is the coefficient A_1 in Equation 1, T_0 is the critical temperature for a normal FE crystal with first-order phase transition features, c takes 0 or 1 to represent a perfect site or a defective site, b_m is the coefficient characterizing the influence of defects on T_0 and can be written as:

$$b_m = -\alpha \frac{dT^0(C_0)}{dC_0} \tag{8}$$

where C_0 is the average concentration of defects, which means that L^2C_0 lattice sites are occupied by defects. In the present model, the unit of temperature is scaled by the energy coefficients that appear in Equation 1. The unit of external electric field E_0 is also scaled by the energy coefficients, considering that Equation 5 has the unit of energy. Therefore, the parameters T, P and E do not have units. A quantitative comparison between the present calculation and experimental data is not allowed in the present work.

For a detailed discussion on the parameter b_m, readers may refer to Ref. [21]. It is assumed that both the sign and magnitude of b_m may be defect-dependent and vary from site to site. Take a defective site i as an example to illustrate how to characterize the role of the defect. If b_m is positive, one expects $A_1(r_i)$ at local site i may be positive, which implies a local stable PE state rather than stable FE state, i.e. the defect will suppress the appearance of a local dipole. A FE state is preferred at site i if $b_m<0$, i.e. the local dipole is enhanced by the defect. The higher the value of $|b_m|$, the more significant the effect of the defect at site i. In the present simulation, the magnitude of b_m is randomly taken within $[0.5b_M, b_M]$ where b_M is the given maximum value of b_m. Here, the two types of defects to be considered in the simulation are characterized by the parameter b_m. For type-I defects, $b_m > 0$ for all defects, i.e. all defects will have a role of suppressing the local dipole. For type-II defects, we define another parameter C_p. $C_pC_0L^2$ sites with defects of $b_m<0$ (enhancing the local dipoles) are imposed randomly to the lattice and $(1-C_p)C_0L^2$ sites with defects of $b_m > 0$ (suppressing the local dipoles) are imposed randomly to the lattice. Of course, one may consider the third case where all defects can enhance the local dipole at the defective sites. However, it is expected that this type of defects plays a role opposite to that of the type-I defects. Thus, this case will not be considered here.

2.3. Monte Carlo simulation

Given a set of system parameters, we first simulate the equilibrium domain configuration of the lattice by employing the Metropolis MC algorithm. Subsequently, we present a discussion on the simulation algorithm of dielectric susceptibility under a weak external electric field. For a lattice, each site is assigned a dipole with moment P being chosen in the range of 0–1.0, and orientation being one of the Q states, respectively. Also, a defect is attached to a site and the probability is determined by C_0. A random number R_1 is generated and a defect is attached to this site if $R_1<C_0$, and is not attached otherwise. Here it should be mentioned that the actual defect concentration in the lattice is slightly smaller than C_0 since the Monte Carlo sequence is statistical. However, since $L = 64$ is large enough the as-induced error in the defect concentration from C_0 is negligible. The simulation begins at an extremely high $T = 14.0$ at which no freezing effect occurs within the period of simulation (we choose $T_0 = 4.0$). For a site i chosen at random, f_L, f_G, f_{dip} and f_E are calculated, respectively, and then the value of H is obtained. Now, this site is assigned another dipole with its moment and orientation taken randomly. Subsequently, H is calculated again to compare with the value of H in the original state, and the difference between them is assumed to be ΔH. A probability p is calculated by the Metropolis algorithm:

$$p = \exp\left(-\frac{\Delta H}{kT}\right) \tag{9}$$

where k is the Boltzmann constant. A second random number R_2 is generated and compared with p. If $R_2<p$, the assumed event above is approved and this dipole at site i is imposed, otherwise, the original state remains unchanged. Then one cycle of simulation is completed and a new cycle is initiated until a given number of cycles has been completed. The time of simulation is scaled by the Monte

Carlo step (*mcs*) and one *mcs* represents $L \times L$ cycles. In our simulation, at each temperature, the initial 600mcs runs are done and then the configuration averaging is performed over the subsequent 2500mcs. Note here that for relaxor systems the short time Monte Carlo simulation can give sufficiently accurate agreement with experiments [8]. The data presented below represent an averaging over four runs with different seeds for random number generator of the initial lattice and defect distribution.

Besides the lattice average polarization and the energy terms as shown in Equations 1–4, one can also evaluate the dielectric susceptibility. The susceptibility is evaluated by applying a weak time-varying external field E of amplitude E_0 and frequency ω: $E = E_0 sin(2\pi\omega \cdot t)$. Since E is time-dependent, the kinetic MC algorithm is performed by the sequence of dipole-exchange between two nearest-neighboring sites with the dipole magnitude determined by the local environment instead of dipole flip sequence employed in the Metropolis algorithm. Such an exchange does not imply any exchange of the defect state. It means the defect distribution in the lattice remains unchanged during the simulation. Under an external ac-electric field E, the lattice dielectric susceptibility χ can be written as [8]:

$$\chi' = \frac{C}{NT}\left\langle \sum_i^N \frac{1}{1+(\omega\cdot\tau/\omega_0)^2} \right\rangle$$
$$\chi'' = \frac{C}{NT}\left\langle \sum_i^N \frac{\omega\cdot\tau/\omega_0}{1+(\omega\cdot\tau/\omega_0)^2} \right\rangle \qquad (10)$$

where $<>$ represents the configuration averaging, χ' and χ'' are the real and imaginary parts of χ (we focus solely on the real part), ω_0 is the polariton frequency which is a material constant, τ is the averaged time for dipole-exchange between any nearest-neighboring dipole-pair, which is scaled by ω_0, $N = L^2$ and C is a temperature-independent constant. In our simulation here, $\omega_0 = 1$ is assumed for simplification. For any dipole-exchange event, the system energy difference ΔH after and before the assumed exchange is calculated and the probability p approving such an exchange is determined by:

$$p = \exp\left(-\frac{\Delta H}{kT}\right) \qquad (11)$$

The simulation is performed by the following procedure. The equilibrium lattice configuration is taken as the input lattice. For a site i, one of its four nearest-neighbors, site j, chosen in random, is paired with site i to perform the dipole-exchange. However, the magnitude of each dipole is re-valued after the assumed exchange. The value of ΔH of this assumed exchange is calculated and the probability for such an exchange is evaluated using Equation 11.

TABLE I System parameters used in the simulation

Parameter	Value	Parameter	Value	Parameter	Value
T_0	4.0	α	1.0	A_{11}	–0.5
A_{12}	9.0	A_{111}	0.8	G_{11}	1.0
G_{14}	0.2	G_{44}	1.0	L	64
b_M	6.0	C_0	0∼1.0	R	8

A random number is generated and compared with this probability to decide whether such an assumed exchange is approved or not. This process is repeated until a given number of simulation steps (*mcs*) is reached. For a site i, if m successful dipole-exchange events are counted in M mcs of simulation, as long as M is big enough, time $\tau = M/m$ because τ is the averaged time for dipole-exchange between any nearest-neighboring dipole-pair. Then the dielectric susceptibility is evaluated using Equation 10.

2.4. Choice of system parameters

In the simulation, b_m and C_0 are treated as variables. The other parameters are chosen and the dimensionless normalization of them is done following the work of Hu *et al.* on $BaTiO_3$ system [26]. Such a choice is somewhat arbitrary since we are not focusing on any realistic system in a quantitative sense. These parameters are given in Table I. In the following simulation, the normal ferroelectric lattice is named as the normal lattice, while the lattice with type-I defects or type-II defects is called the defective lattice.

3. Lattice dipole configuration of normal lattice

3.1. Lattice configuration at $Q = 4$

We first look at the simulated dipole configuration of the normal lattice ($C_0 = 0.0$). Fig. 2 shows the simulated patterns at several temperatures for $Q = 4$, where the length and direction of arrows represent the moment and orientation of dipoles. For a clarification of the dipole alignment, only part of each lattice is shown. At high $T = 12.0$ and 6.0, the moment of all dipoles is very small and their alignment is disordered, a typical PE configuration. As T becomes close to T_0 ($T = 4.0$), the dipole moment is still small and no long-range dipole order is found either, although a small dipole-ordered region is observed on the top-right corner.

Once T is below T_0 ($T = 3.0$), the ferroelectric phase transition occurs and the disordered dipole alignment evolves into a long-range ordered structure. A clear ferroelectric multi-domain configuration is formed with the well-predicted head-to-tail dipole alignment and preferred 90° domain walls. Those dipoles on the domain walls are still small in moment and their alignment remains partially disordered. At a low T ($T = 1.0$), the degree of disordering on the walls is significantly suppressed and an almost perfect multi-domain lattice is observed.

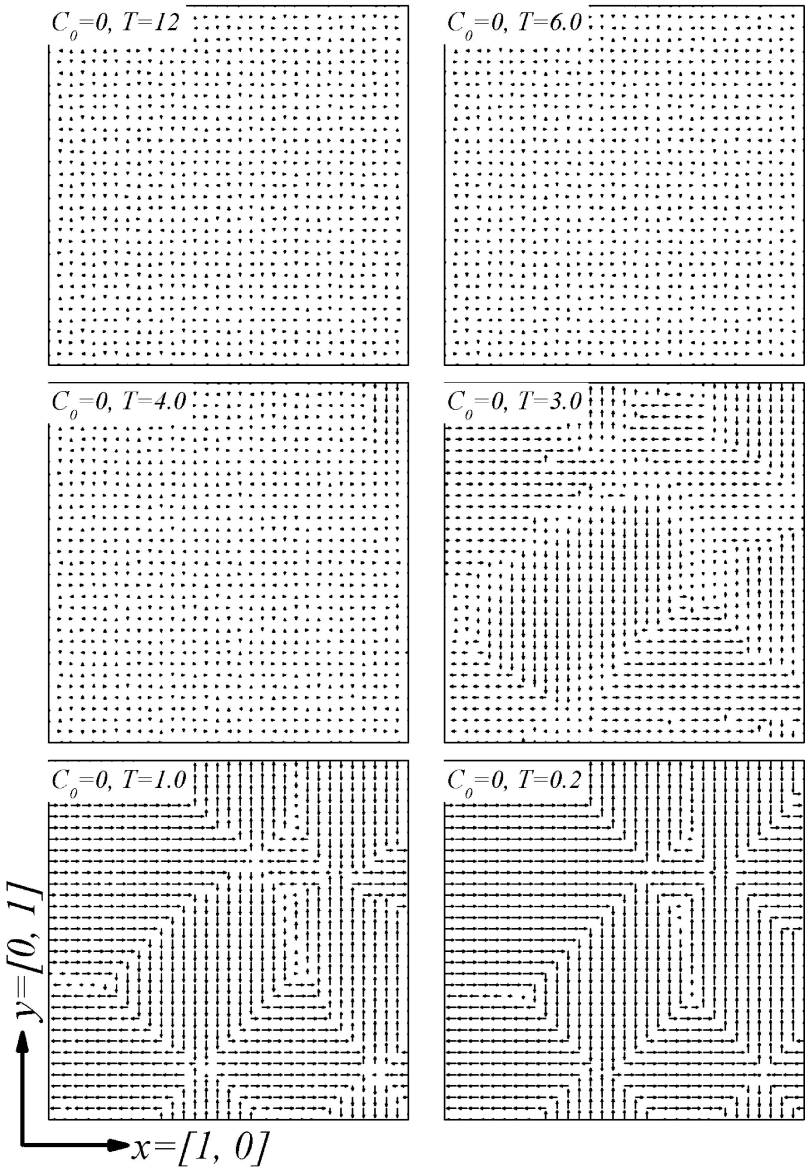

Figure 2 Simulated dipole configuration of normal ferroelectric lattice at different temperatures T ($Q = 4$). $C_0 = 0$.

As for the domain configuration, one may find that most of the domains are 90°-type rather than 180°-type. However, in the dipole configurations shown above, the 180°-domain walls are still observed. One reason for less 180°-domain walls may be due to the energy landscape in which the 90°-walls are preferred than the 180°-walls in the present model. In fact, if smaller G_{11}, G_{12}, G_{44} and G'_{44} are chosen so that a smaller f_G is obtained, i.e. lower domain wall gradient energy is imposed, many more 180°-walls than 90°-walls are observable.

3.2. Lattice configuration at $Q > 4$

When the allowed number of dipole orientations $Q > 4$, the lattice configuration is also simulated, and the simulated dipole alignment patterns at $T = 0.5$ are presented in Fig. 3 ($Q = 4, 8, 16$). For all cases, the lattice is completely disordered at $T > T_0$, i.e. the lattice is in the paraelectric state and all the allowed states of dipole orientation are chosen (patterns not shown here). While almost the same domain pattern is shown for lattices of different Q, the dipole alignment on the 90°-walls is Q-dependent. At $Q = 4$, the 90°-wall is almost perfect with the head-to-tail dipoles aligning perpendicular to each other. For $Q = 8$, most dipoles on the walls have [11] orientations instead of [1,0] or [0,1] orientations. We name these alignment states the distorted states while the four ±[1,0] and ±[0,1] states are viewed as normal states. At $Q = 16$, almost all dipoles on the walls deviate from the [1,0] and [0,1] orientations and prefer the distorted states which have a higher f_L. Therefore, in the Ginzburg-Landau model the four ±[1,0] and ±[0,1]

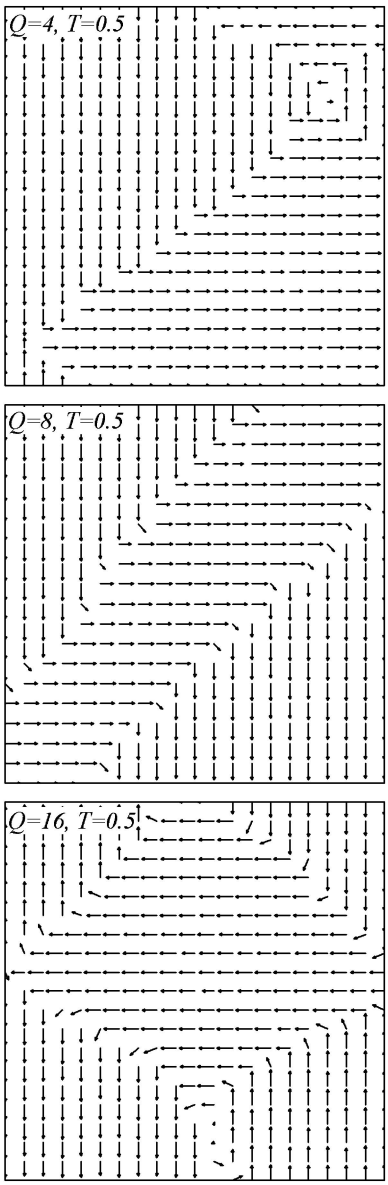

Figure 3 Simulated dipole configuration of normal ferroelectric lattices with different values of Q at $T = 0.5$. $C_0 = 0$.

orientations ($Q = 4$) may not be the unique choices for the dipoles.

As shown above, all dipoles except those on the walls still take one of the four ±[1,0] and ±[0,1] orientations no matter how large the value of Q is in the simulation. This behavior can be explained by the symmetry of the Landau potential Equation 1. With the parameters given in Table I, we calculate the Landau potential F_{ld} as a function of (P_x, P_y) at $T = 0.5$ and $T = 5.0$, as shown in Fig. 4a and b, respectively. The square symmetry of $F_{ld}(P_x, P_y)$ at low T, characterized by the four symmetric energy minimals, is clearly shown, which is independent of Q. The result implies that the preferred dipole orientation states are ±[0,1] and ±[1,0] irrespective of the value of Q. At high T, $F_{ld}(P_x, P_y)$ still shows the square symmetry although the energy minimum is located at the zero-point ($P_x = P_y = 0$), i.e. the lattice is in the paraelectric state.

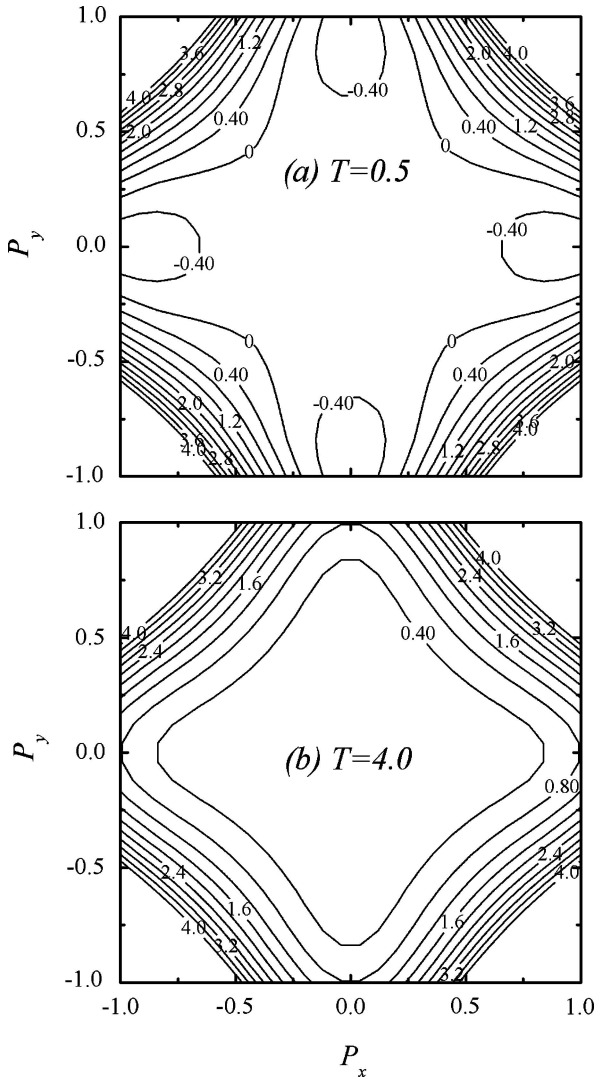

Figure 4 Equi-potential contour of the Landau potential f_L as a function of the dipole moment components P_x and P_y at (a) $T = 0.5$ and (b) $T = 4.0$. The numbers inserted in the plots are the values of f_L.

In the following simulation for the defective lattice, we fix $Q = 4$ and the effect of varying Q is no longer taken into account.

4. Dipole configuration in defective lattices

4.1. Dipole configuration in a lattice with type-I defects

We look at the dipole alignment in the lattice at different T for $C_0 = 0.5$ and $C_p = 0.0$ (with type-I defects), as shown in Fig. 5. The type-I defects intrinsically suppress the local dipoles. At high T, the lattice is obviously in the PE state and no long-range ordered dipole alignment is seen. With decreasing T, the lattice becomes inhomogeneous

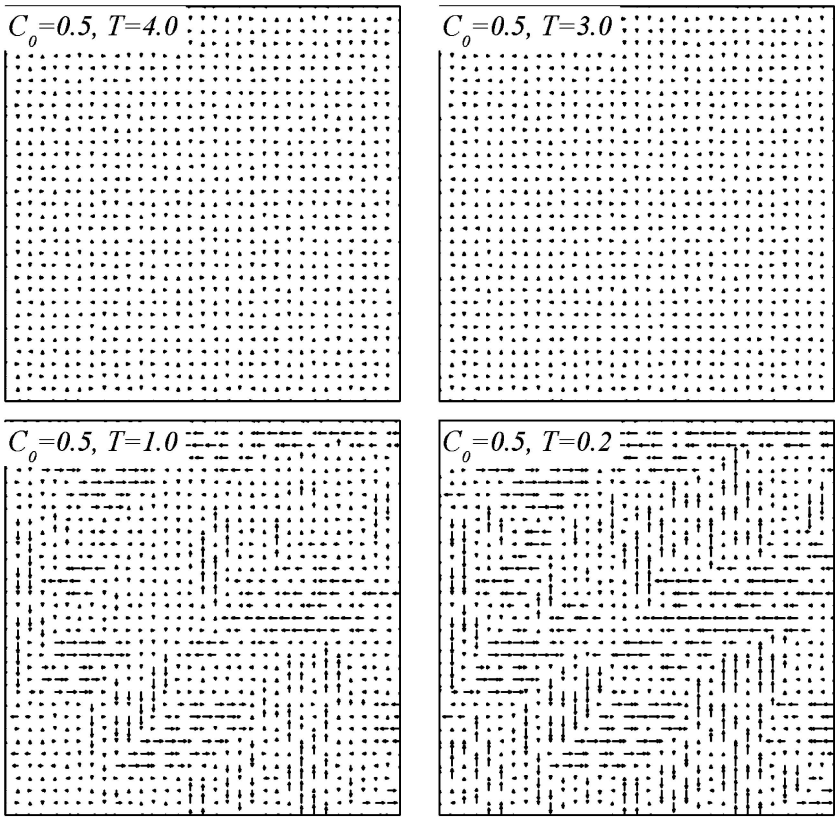

Figure 5 Simulated dipole configuration of a ferroelectric lattice with type-I defects at different temperatures T ($C_0 = 0.5$, $C_p = 0.0$, $Q = 4$). The values of T are inserted in figures.

and some FE ordered regions are observed. With further decreasing of T, these FE ordered regions grow in size and new FE regions appear. At low T, the lattice has a two-phase coexisted microstructure consisting of FE phase embedded in the matrix of PE phase, a typical picture for RFEs.

Given a temperature $T = 1.0$, the lattice dipole configuration with increasing C_0 is shown in Fig. 6. For a small C_0 ($C_0 = 0.2$), the lattice inhomogeneity is already remarkable and the decrease in moment (depolarization effect) of the dipoles along the domain walls becomes significant although the defects are randomly distributed. These regions can be viewed as the non-ferroelectric phase or simply the PE phase. With increasing C_0, the FE regions continue to shrink both in size and in volume fraction. It is seen that only very small dipole clusters exist at $C_0 = 0.5$. As $C_0 = 0.8$, the FE phase in the lattice nearly disappears and the whole lattice becomes paraelectric.

4.2. Dipole configuration in a lattice type-II defects

When type-II defects are introduced into the normal lattice, one sees a dipole configuration quite different from that of the type-I defects. The simulated dipole alignment patterns for $C_0 = 0.5$ ($C_p = 0.5$) at different temperatures are shown in Fig. 7. We indeed find that there are some small-sized areas in which the dipole alignment is ordered at $T = 6.0$, i.e. some local clusters of ordered dipoles form at $T > T_0$. At $T = 4.0$, this clustering tendency becomes more significant. The number and size of the clusters increase with decreasing T. On the other hand, at T just below T_0, we do not see a perfect long-range ordered dipole configuration, while the lattice still consists of areas of ordered dipoles embedded in a matrix of paraelectric phase. With further decreasing of T, a gradual growth and coalescence of these ordered clusters is observed, and the simulated lattice at very low temperature has a configuration approaching that of a normal ferroelectric.

Obviously, the main configuration features described above are similar to those of RFEs in which nano-polar clusters are embedded in a PE matrix over a wide range of temperature both above and below T_0. The feature of diffusive phase transition is clearly reproduced, indicating that the present model works well in describing the microstructure of RFEs. It should be mentioned that in Fig. 7 the long-range ordered configuration is already well developed as T falls to $T = 1.0$, at which a well-defined domain pattern can be identified although there still are some small dipole-disordered zones inside the domains. This configuration can be viewed as the frozen one, which

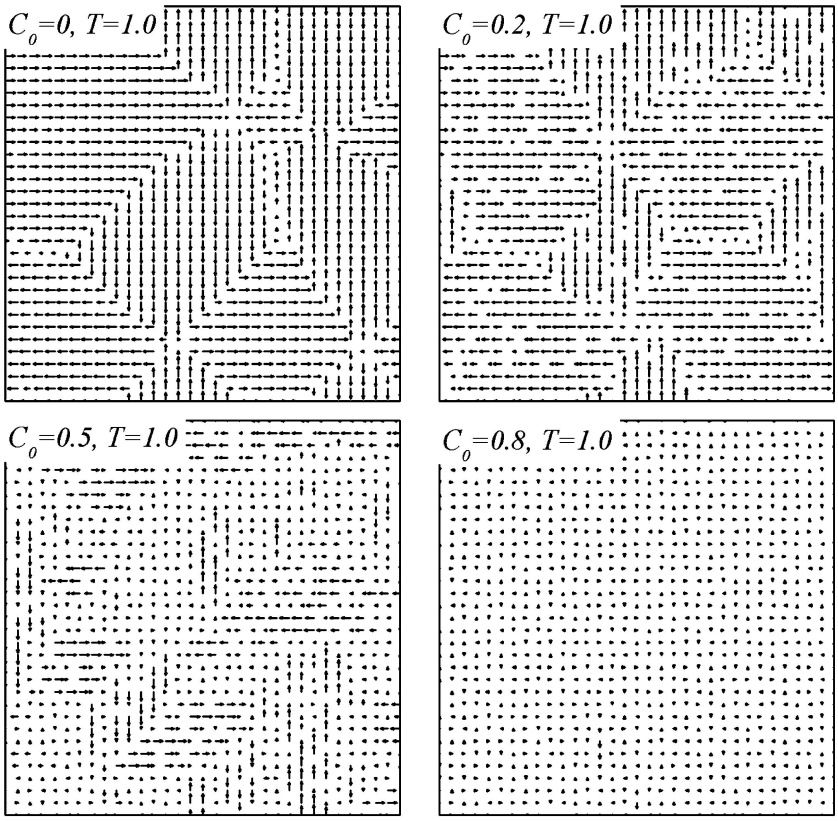

Figure 6 Simulated dipole configuration of a ferroelectric lattice with type-I defects at different defect concentrations C_0 ($T = 1.0$, $C_p = 0.0$, $Q = 4$). The values of C_0 are inserted in the figures.

reflects somehow the freezing behavior of relaxor ferroelectrics with decreasing temperature [21]. However, this freezing behavior is C_0-dependent and the long-range ordered domains disappear when C_0 is high. We simulate the evolution of dipole configuration with different C_0, as shown in Fig. 8 ($T = 3.0$). Multi-domain configuration is clearly seen at $C_0 = 0.0$ and 0.2, but is no longer visible at $C_0 = 0.5$ and 0.8. Consequently, when C_0 becomes larger, the ferroelectric transition is not completed unless T is lower. At any given temperature, the larger the value of C_0, the smaller the ordered clusters.

5. Ferroelectric and dielectric behaviors of defective lattice

5.1. Ferroelectric behaviors

We also study the ferroelectric behaviors of the lattices with the two types of defects, as a function of T and E. The external field was fixed at $\omega = 0.002$ mcs^{-1} and $E_0 = 4.0$ for the simulations in this section. For the lattice with type-I defects, the simulated P-E hysteresis loops at $T = 3.0$ for different C_0 are presented in Fig. 9a. It is seen that the loop shrinks significantly along the P- and E-axis as C_0 increases. At $C_0 = 0.8$ and 1.0, the hysteresis loop becomes very thin, a typical feature of RFEs at a temperature slightly below T_0. Because the loop area A represents the energy dissipated during one cycle of domain reversal driven by the ac-electric field, it can be used to scale the long-range correlation of dipoles in the lattice. In Fig. 9b, the loop area A as a function of T at various C_0 is shown. Given the value of C_0, A increases rapidly with decreasing T, while for a given T, A decreases with increasing C_0. These results are consistent with the behaviors of RFEs.

Nevertheless, for lattices with type-II defects, the simulated ferroelectric behaviors are very different, as shown in Fig. 10a where the P-E hysteresis loops for different C_0 at $T = 3.0$ are given, and in Fig. 10b where the loop area A for different C_0 as a function of T is plotted. As C_0 ($C_p = 0.5$) varies over a broad range, the simulated hysteresis loop does not change much but only shrinks slightly along the P- and E-axis. Even at $C_0 = 1.0$, the lattice polarization P still has a large value. In Fig. 10b, the loop area for $C_0 > 0$ is slightly larger than that for the normal FE lattice at $T > T_0$, although it is slightly smaller than that for the normal FE lattice at $T < T_0$.

The significant difference in ferroelectric behaviors between the lattices with the two different types of defects originates from the fact that, for the lattice with type-II defects, half of the defects enhance the local dipole moment, while for the lattice with type-I defects all defects suppress the local dipole moments. Therefore, for the

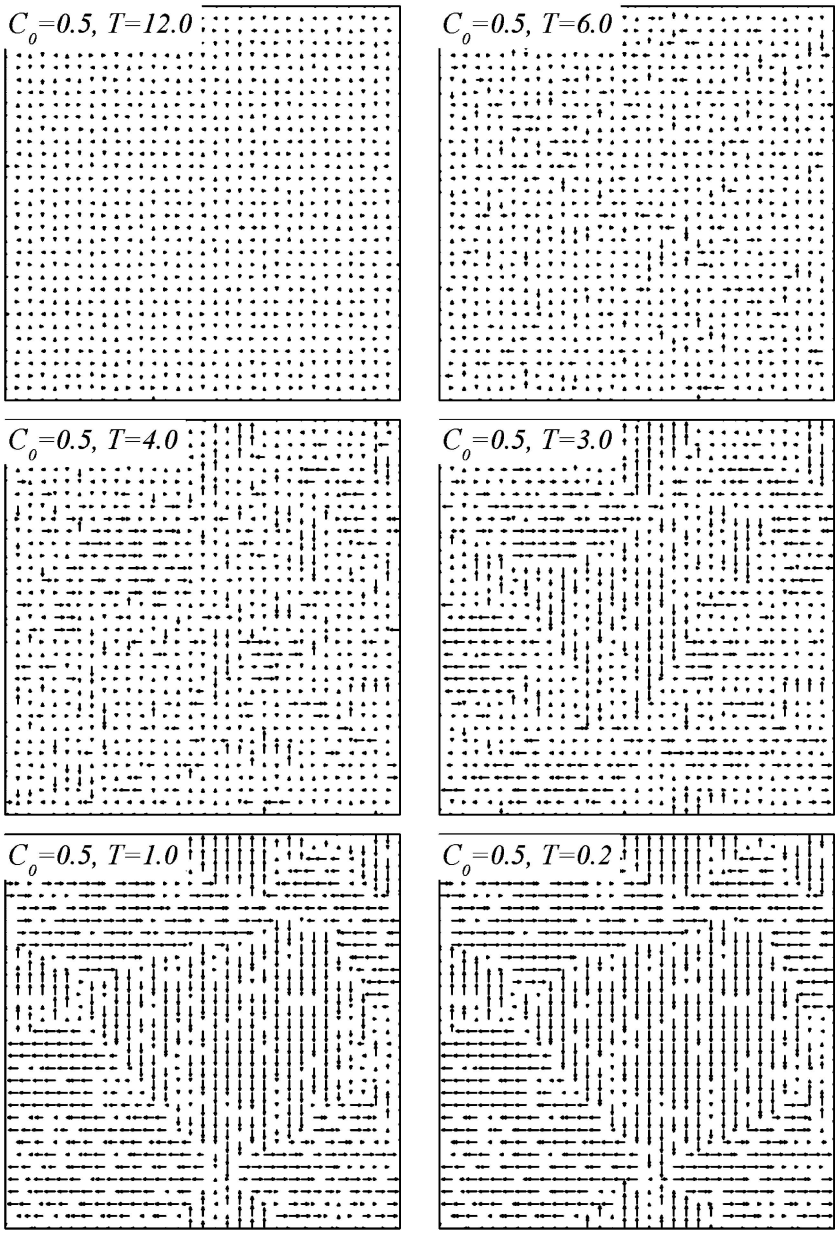

Figure 7 Simulated dipole configuration of a ferroelectric lattice with type-II defects at different temperatures T ($C_0 = 0.5$, $C_p = 0.5$, $Q = 4$). The values of T are inserted in figures.

lattice with type-II defects, some defective sites exhibit even larger dipole moments than those of the normal FE lattice sites at $T>T_0$, although the other sites exhibit smaller dipole moments, as shown in Fig. 8. These results indicate that most RFEs studied experimentally are doped with type-I defects which intrinsically suppress the local dipole moments. This argument will gain further support below in the discussion of the dielectric behavior.

5.2. Dielectric behaviors

The dielectric susceptibility χ as a function of T for different C_0 under a given E ($\omega = 0.002mcs^{-1}$, $E_0 = 4.0$) for lattices with the two types of defects is evaluated, and the results are plotted in Fig. 11a (lattice with type-I defects) and 11b (lattice with type-II defects, $C_p = 0.5$), respectively. It is seen that the introduction of defects affects significantly the dielectric property of the system. At $C_0 = 0$ (normal FE), a Curie-Weiss type single-peaked χ-T relation is generated with T_c~4.0. For the lattice with type-I defects, as C_0 increases, the single-peaked χ-T curve shifts toward the low-T side and also downwards slightly. In addition, the normal FE lattice shows a sharp decrease in χ at a temperature just below T_c, but this feature is weakened for the lattice with defects, i.e. the FE transition becomes diffused with increasing C_0. For the

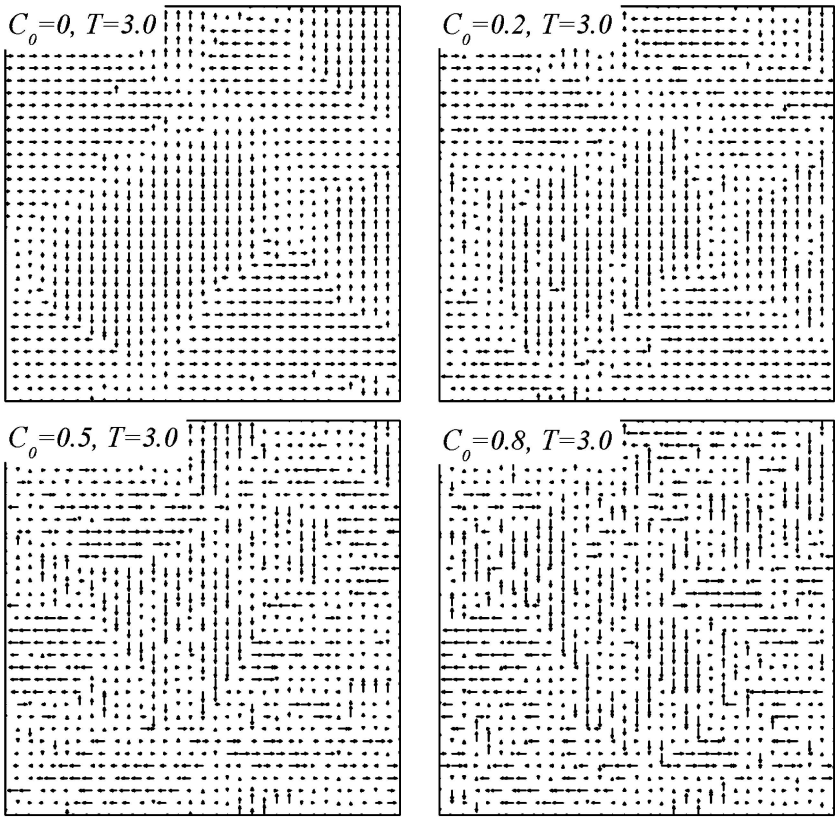

Figure 8 Simulated dipole configuration of a ferroelectric lattice with type-II defects at different defect concentrations C_0 ($T = 1.0$, $C_p = 0.5$, $Q = 4$). The values of C_0 are inserted in the figures.

lattice with type-II defects, with increasing C_0, one sees a remarkable broadening of the dielectric peak around the transition point and the peak position shifts slightly toward the high-T side. Over the high temperature range ($T>T_0$), χ' decreases slightly with increasing C_0, while over the low T range ($T<T_0$) it increases slightly with C_0. When C_0 is extremely large ($C_0 = 1.0$), which means all lattice sites are occupied by the defects, χ' does not exhibit a peak around the transition point and it decreases monotonously with decreasing T. This behavior has never been observed experimentally and its significance is in doubt. Therefore, it is believed that most RFEs under conventional investigations are doped with type-I defects. Finally, the dielectric behaviors for the two-types of defective lattices can be explained qualitatively by considering the energy terms as a function of defect concentration and details of the explanation can be found elsewhere [22, 23].

5.3. Comparison with experiments

We have employed the defect model to simulate the dipole configuration for lattices with two types of randomly distributed defects. A qualitative comparison of these simulated behaviors with experimental data would help provide a justification for the defect model. It has been repeatedly verified that tremendous variations in microstructure and physical property of a variety of ferroelectric polymers may be generated by irradiation with high energy electrons or protons [18–20, 25]. Several experiments revealed that the high-energy particles injected into the copolymers convert the single FE-phase into a two-phase coexisted microstructure with a FE phase and a PE phase. In fact, one may argue that the high energy particle irradiation introduces randomly distributed point-like defects into the sample and disrupts the stability of the FE phase. The microstructural details are determined by the energy level and the dose of the particles. At a given energy level, the defect concentration C_0 is directly related to the dose of irradiation.

The above argument provides justification for the application of the present model to explain the results of the irradiation experiments. While several careful experiments on the effect of irradiation had been performed, in this section, we compare our model simulation with our earlier experiments on the dielectric susceptibility of proton-irradiated poly (vinylidene fluoride-trifluoroethylene) 70/30 mol% copolymer (P(VDF-TrFE)). For details of the experiments, please refer to our earlier report [25].

Fig. 11c shows the measured dielectric constant at 1MHz as a function of T in a cooling run for several samples with the same initial state but irradiated at

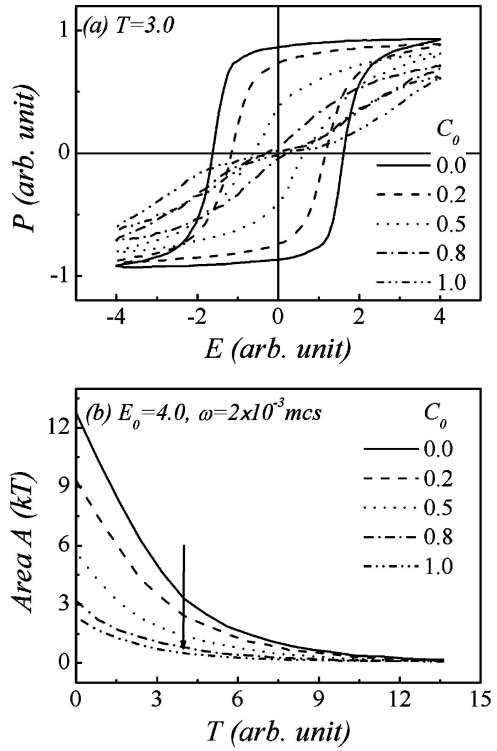

Figure 9 (a) Simulated ferroelectric hysteresis loops for a lattice with type-I defects at different defect concentrations C_0, (b) loop area A at different defect concentrations C_0 as a function of temperature T. $E_0 = 4.0$ and $\omega = 0.002$ mcs^{-1}.

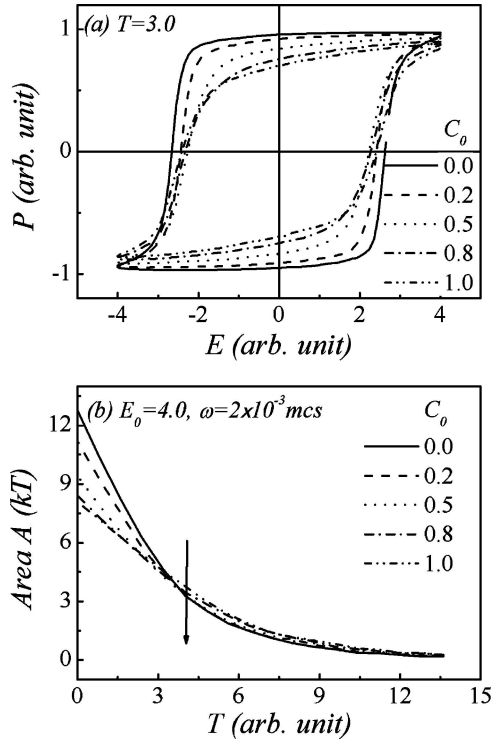

Figure 10 (a) Simulated ferroelectric hysteresis loops for a lattice with type-II defects at different defect concentrations C_0, (b) loop area A at different defect concentration C_0 as a function of temperature T. $C_p = 0.5$, $E_0 = 4.0$ and $\omega = 0.002$ mcs^{-1}.

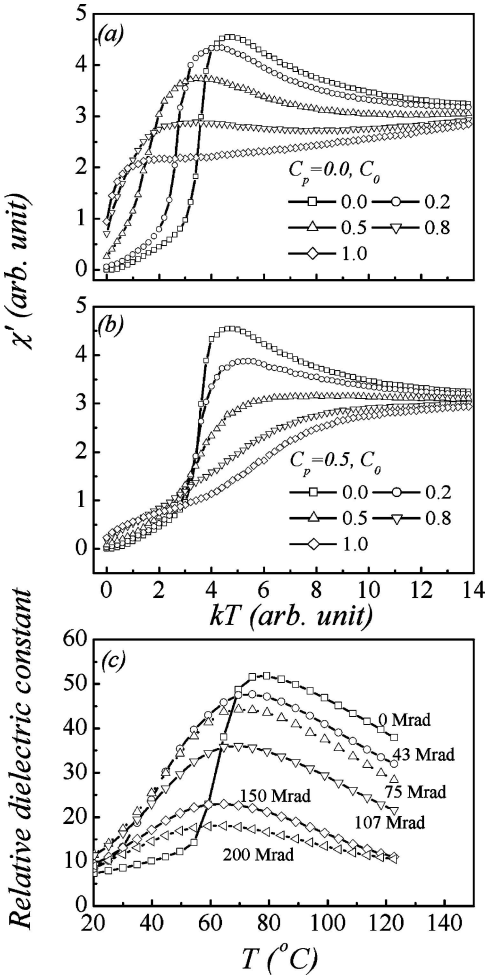

Figure 11 Simulated dielectric susceptibility χ' as a function of temperature T at different defect concentration C_0, for (a) lattice with type-I defects and (b) lattice with type-II defects ($E_0 = 4.0$ and $\omega = 0.002$ mcs^{-1}), and (c) relative dielectric permittivity χ measured at 1 MHz as a function of temperature T for P(VDF-TrFE) 70/30 mol% copolymer samples irradiated with different proton doses in a cooling run.

different dose levels. While the non-irradiated sample shows the typical first-order FE phase transitions at 70°C, the irradiated samples exhibit a broader transition peak and the peak height becomes smaller and the peak position shifts to a lower T, as the irradiation dose increases. These features are well reproduced in our simulations on the lattice with type-I defects, as shown in Fig. 11a. In fact, hysteresis measurements indicated that a relaxor-like two-phase microstructure is formed in irradiated ferroelectric copolymers, and the measured hysteresis loops are quite similar to the simulated ones shown in Fig. 9. What should be mentioned here is that the shift of the peak position becomes quite small when the dose is higher than 150Mrad and this is not consistent with our simulations where a significant shift continues at a very high defect concentration ($C_0 > 0.6$).

6. Conclusions

In conclusion, we have presented a Monte Carlo simulation on the dielectric and ferroelectric properties of ferroelectric lattices with two-types of randomly distributed point-like defects and compared the simulated results with the properties of proton-irradiated copolymer (P(VDF-TrFE)). The algorithm of simulation is based on the Ginzburg-Landau theory for first-order ferroelectric phase transition with the inclusion of the contributions from dipole-dipole interaction, gradient energy and electrostatic energy. The simulation has revealed that the introduction of the two types of lattice defects results in an evolution of the dipole configuration from a normal multi-domain ferroelectric lattice to a relaxor-like two-phase coexisted microstructure consisting of ferroelectric regions embedded in the matrix of a paraelectric phase. The dielectric susceptibility as a function of defect concentration has been simulated and the simulated results are very similar to those observed for relaxor ferroelectrics.

Acknowledgment

This work is supported by the 973 Project of China (2002CB613303) and NSFC Project of China (10021001, 50332020, 10474039), the Centre for Smart Materials of the Hong Kong Polytechnic University and the Hong Kong Research Grants Council (PolyU 5147/02E).

References

1. M. E. LINES and A. M. GLASSS, "Principles and applications of ferroelectrics and related materials" (Gordon and Breach, New York, 1977).
2. I. S. ZHELUDEV, in "Solid State Physics," edited by H. Ehrenreich, F. Seitz and D. Turnbull (Academic Press, New York, 1971) Vol. 26, p. 429.
3. L. E. CROSS, *Ferroelectrics* **76** (1987) 241.
4. A. P. LEVANYUK and A. S. SIGOV, *Defects and structural phase transitions* (Gordon and Breach, New York, 1988).
5. N. ICHINOSE, *Ferroelectrics* **203** (1997) 187.
6. Q. M. ZHANG, J. ZHAO, T. R. SHROUT and L. E. CROSS, *J. Mater. Res.* **12** (1997) 1777.
7. C. H. PARK and D. J. CHADI, *Phys. Rev. B.* **57** (1998) 13961.
8. Z. WU, W. DUAN, Y. WANG, B. L. GU and X. W. ZHANG, *ibid.* **67** (2003) 052101.
9. B. E. VUGMEISTER and M. D. GLINCHUK, *Rev. Mod. Phys.* **62** (1990) 993.
10. E. COURTENS, *Phys. Rev. Lett.* **52** (1984) 69.
11. A. K. TAGANTSEV, *ibid.* **72** (1994) 1100.
12. C. C. SU, B. VUGMEISTER and A. G. KHACHATURYAN, *J. Appl. Phys.* **90** (2001) 6345.
13. R. FISCH, *Phys. Rev. B.* **67** (2003) 094110.
14. D. VIEHLAND, S. J. JANG and L. E. CROSS, *J. Appl. Phys.* **68** (1990) 2916.
15. C. RANDALL, D. J. BARBER, R. W. WHATMORE and P. GROVES, *J. Mater. Sci.* **21** (1987) 4456.
16. X. H. DAI, Z. XU and D. VIEHLAND, *Philos. Mag. B.* **70** (1994) 33.
17. G. Smolenski and A. Agranovska, *Sov. Phys. Solid State* **1** (1960) 1429.
18. A. J. LOVINGER, *Macromolecules* **18** (1985) 910.
19. B. DAUDIN, M. DUBUS, F. MACCHI and L. F. LEGRAND, *Nucl. Inst. Meth. Phys. Res. B* **32** (1988) 177.
20. Q. M. ZHANG, V. BHARTI and X. ZHAO, *Science* **280** (1998) 2101.
21. S. SEMENOVSKAYA and A. G. KHACHATURYAN, *J. Appl. Phys.* **83** (1998) 5125.
22. J.-M. LIU, X. WANG, H. L. W. CHAN and C. L. CHOY, *Phys. Rev. B.***69** (2004) 094114.
23. X. WANG, J.-M. LIU, H. L. W. CHAN and C. L. CHOY, *J. Appl. Phys.* **95** (2004) 4282.
24. J.-M. LIU, K. F. WANG, S. T. LAU, H. L. W. CHAN and C. L. CHOY, *Comput. Mater. Sci.* **33** (2005) 66.
25. S. T. LAU, H. L. W. CHAN and C. L. CHOY, *Appl. Phys. A* **80** (2005) 289–294.
26. H. L. HU and L. Q. CHEN, *Mater. Sci. & Eng. A* **238** (1997) 182; *J. Am. Ceram. Soc.* **81** (1998) 492.